

Effect of terminal velocities on macroscopic and microscopic hydrodynamic mixing of stratified suspensions

Yasufumi Yamamoto¹* and Ryoko Otomo²

Department of Mechanical Engineering, Kansai University 3-35, Yamate-cho 3-chome, Suita, Osaka 564-8680, Japan

Yohsuke Tanaka³

Faculty of Mechanical Engineering, Kyoto Institute of Technology, Matsugasaki, Sakyo-ku, Kyoto 606-8585, Japan

Shusaku Harada⁴

Division of Sustainable Resources Engineering, Faculty of Engineering, Hokkaido University, N13-W8, Sapporo, Hokkaido 060-8628, Japan

 (Received 9 June 2022; revised 26 August 2022; accepted 2 October 2022; published 24 October 2022)

We performed numerical experiments to investigate the mixing of stratified suspensions composed of different particle types by gravitational sedimentation. The mixing process is controlled by a dimensionless group $Y_m \sim U_f/U_{St1}$, where U_f is a typical velocity of a macroscopic sedimenting finger and U_{St1} is the Stokes settling velocity of a single spherical particle in the upper suspension. The effects of components of Y_m , in particular, terminal velocities of particles, were investigated. For $Y_m = 100$, no large difference was observed for the difference of components of Y_m , and it was confirmed that the mixing rate is determined by Y_m , because macroscopic (vessel-scale) mixing is dominant for large Y_m . For $Y_m = 5$, macroscopic mixing and microscopic (individual particle-level) mixing due to the particle terminal velocity difference are of the same order, while completely different mixing patterns were observed for positive, zero, and negative terminal velocity differences: macroscopic mixing is promoted by the increase in apparent density due to microscopic mixing, small macroscopic mixing is suppressed by the individual particle settling, and jetting mixing occurs owing to pure liquid layer formation.

DOI: [10.1103/PhysRevE.106.045109](https://doi.org/10.1103/PhysRevE.106.045109)

I. INTRODUCTION

The mixing of solid particles suspended in liquids is important not only in engineering processes related to pastes and slurries but also in global natural phenomena such as the formation of sedimentary layers [1]. If the gravity force is significant, i.e., if the mixing occurs during sedimentation, the relative motions of particles at various length-scales are caused by the hydrodynamic interaction between particles [2,3] and the relative motion plays an important role in the mixing. Therefore, such mixing processes should be treated as hydrodynamic events rather than thermodynamic ones, such as an increase in mixing entropy.

Hydrodynamic mixing of stratified particle suspensions with different conditions is further complicated by a combination of hydrodynamic interactions and the effect of gravity. For example, the settling velocity varies with the particle concentration because of hydrodynamic interactions [4]. Furthermore, large-scale convection occurs occasionally by interfacial instability (Rayleigh-Taylor instability) at the boundary of a suspension (concentration interface), and particles settle collectively [5–7]. Consequently, particle relative motions of various spatial scales can occur at the concentration interface with different suspension conditions. Therefore, the hydrodynamic mixing of particles is complex, involving

not only the physical properties of suspended particles but also the collective nature of the particles and the characteristics of gravitational instability occurring at the concentration interface.

The miscible or immiscible nature of the concentration interface of fine particles is determined by the flow induced by individual particles [8–10], which differs from the ordinary fluid interface. When the particle concentration is large enough, the interface exhibits an immiscible nature; on the contrary, when the concentration is low, the immiscibility of the interface is no longer maintained, and other particles from the outside are allowed to enter. Mori *et al.* [11] conducted experiments and numerical analyses of how particles mix at the concentration interface of suspensions with different concentrations. They found that “collectivity” (its definition is described later) is important for the mixing behavior and that the settling velocity of the upper suspension is proportional to the difference between the squares of the modified collectivities of the upper and lower suspensions. Yamamoto *et al.* [12] performed numerical experiments in which the upper and lower suspensions were composed of different types of particles. The results showed that the difference between the collectivities of the upper and lower suspensions causes mixing at the particle scale (microscopic mixing) and vessel-scale collective mixing (macroscopic mixing).

Yamamoto *et al.* [12] found that the mixing rate of stratified suspensions of low-Reynolds-number particles in a narrow-depth vessel by gravity by the following simple theoretical

*yamayas@kansai-u.ac.jp

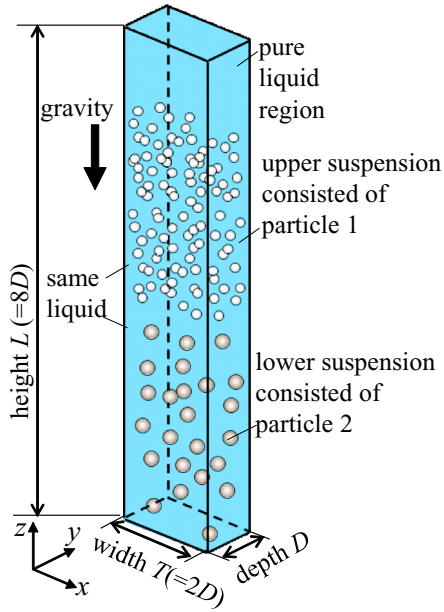


FIG. 1. Configuration of stratified suspensions in a rectangular vessel.

consideration. First, the Stokes terminal velocity of a single particle, U_{St} , is given as

$$U_{St} = \frac{(\rho_p - \rho_l)}{18\mu_1} d_p^2 g, \quad (1)$$

where ρ_p and ρ_l denote the particle and liquid mass density, respectively, μ_1 denotes the dynamic viscosity of the liquid, d_p is the particle diameter, and g is the gravitational acceleration. Assuming that the settling finger is immiscible, the finger's settling velocity U_f can be given in the form of the Hadamard-Rybczynski solution [13] or the single-mode Rayleigh-Taylor bubbling velocity [14,15] as

$$U_f = K' \frac{(\rho_{s1} - \rho_{s2})}{\mu_1} D^2 g, \quad (2)$$

where the typical length of the finger is taken as the vessel depth D , K' is a constant, which is determined on the basis of the vessel configuration, and ρ_s is the apparent mass density of the suspension. Subscripts 1 and 2 represent the upper and lower suspensions, respectively, throughout this paper. ρ_{s1} is represented as

$$\rho_{s1} = \phi_1 \rho_{p1} + (1 - \phi_1) \rho_l = \phi_1 (\rho_{p1} - \rho_l) + \rho_l, \quad (3)$$

where ϕ is the volume fraction of particles and ρ_{s2} is given in a similar form. Then, the nondimensional finger's settling velocity can be calculated as follows [noting the factor of Eq. (1)]:

$$\begin{aligned} \frac{U_f}{U_{St1}} &= \frac{K'}{U_{St1}} \frac{\phi_1 (\rho_{p1} - \rho_l) - \phi_2 (\rho_{p2} - \rho_l)}{\mu_1} D^2 g \\ &= 18K' \left[\frac{1}{U_{St1}} \frac{(\rho_{p1} - \rho_l)}{18\mu_1} d_{p1}^2 g \left(\frac{D}{d_{p1}} \phi_1^{1/2} \right)^2 \right. \\ &\quad \left. - \frac{1}{U_{St1}} \frac{(\rho_{p2} - \rho_l)}{18\mu_1} d_{p2}^2 g \left(\frac{D}{d_{p2}} \phi_2^{1/2} \right)^2 \right] \\ &= KY_m, \end{aligned} \quad (4)$$

where $K = 18K'$. Y_m is defined as follows:

$$Y_m = C_{\text{mod1}}^2 - \frac{U_{St2}}{U_{St1}} C_{\text{mod2}}^2, \quad (5)$$

where C_{mod} is the modified collectivity of suspension, as discussed in Mori *et al.* [11],

$$C_{\text{mod}} = \frac{D}{d_p} \phi^{1/2}. \quad (6)$$

The original ‘‘collectivity’’ C is defined as

$$C = \frac{D}{d_p} \phi^{1/3}. \quad (7)$$

C represents the ratio of the macroscopic finger scale to the mean distance of particles, namely, the resolution of the finger by Stokeslets. Y_m represents the index of gravity instability because it is proportional to the apparent density differences. Furthermore, Y_m contains the terminal velocities of the upper and lower particles, so the effect of differential settling is contained in Y_m .

In this study, we define the mixing length Z_{mix} of the stratified suspension due to gravitational settling as the vertical distance between the bottom-most particle of the upper suspension and the top-most particle of the lower suspension, as reported by Yamamoto *et al.* [12], and examine the mixing rate dZ_{mix}/dt . For gravitationally stable conditions ($\rho_{s1} \leq \rho_{s2}$) corresponding to $Y_m \leq 0$ [found from Eqs. (2) and (4)], the mixing only occurs due to the particle terminal velocity difference $U_{St1} > U_{St2}$. We call the mixing behavior due to the terminal velocity difference ‘‘microscopic mixing,’’ and the mixing rate can be estimated as $U_{St1} - U_{St2}$. On the other hand, for gravitationally unstable conditions ($\rho_{s1} > \rho_{s2}$)

TABLE I. Suspension conditions for test 1. Subscripts 1 and 2 represent upper and lower suspensions, respectively.

Case	Y_m	Mod. collect.		Diam. (μm)		Part. density (kg/m^3)		Vol. frac.		Susp. density (kg/m^3)		Term. vel. U_{St2}/U_{St1}
		C_{mod1}	C_{mod2}	d_{p1}	d_{p2}	ρ_{p1}	ρ_{p2}	ϕ_1	ϕ_2	ρ_{s1}	ρ_{s2}	
1-A- α	100	11.00	4.58	33.4	29.3	7557	9528	0.015	0.002	1074	992	1
1-A- β				80.2		2116.58		0.015	0.015			
1-B- α	100	14.00	9.79	30.3	21.7	8972	16567	0.02	0.005	1135	1053	1
1-B- β				43.3		4891		0.02	0.02			
1-C- α	100	20.2	17.32	33.5	24.5	7517	13206	0.05	0.02	1302	1220	1
1-C- β				38.7		5877		0.05	0.05			

TABLE II. Suspension conditions for test 2. Subscripts 1 and 2 represent upper and lower suspensions, respectively.

	Y_m	C_{mod1}	C_{mod2}	d_{p1}	d_{p2}	ρ_{p1}	ρ_{p2}	ϕ_1	ϕ_2	ρ_{s1}	ρ_{s2}	$U_{\text{St2}}/U_{\text{St1}}$
2-A- α	100	11.00	3.24	33.4	29.3	7557	18080	0.015	0.001	1074	992	2
2-A- β					80.2		3258		0.0075			
2-B- α	100	Identical to 1-A- α						0.015	0.004	1074	992	0.5
2-B- β		Identical to 1-A- β										
2-C- α	100	11.00	6.48	33.4	29.3	7557	5251	0.015	0.004	1074	992	0.5
2-C- β					80.2		1546		0.03			

corresponding to $Y_m > 0$, Rayleigh-Taylor mixing occurs with fingering settling. In this case, we call the mixing behavior “macroscopic mixing,” and the mixing rate can be estimated by twice the finger’s settling speed [12]:

$$\frac{dZ_{\text{mix}}}{dt} \frac{1}{U_{\text{St1}}} = 2KY_m. \quad (8)$$

Further, if particle terminal velocities differ between the upper and lower suspensions, both microscopic and macroscopic mixing can simultaneously occur. However, as pointed out by previous works [7,11,12,16], the finger’s settling speed is much larger than the single particle terminal velocity. Thus, under gravitationally unstable conditions, microscopic mixing cannot be found in many cases.

In this work, we describe the mixing behaviors of stratified suspensions with small and high Y_m numbers with varying collectivities and particle terminal velocities, which are the components of Y_m in Eq. (5). In particular, we observe the mixing behaviors of the cases with a small macroscopic mixing rate in the order of the individual particle terminal velocity in detail.

II. SYSTEM AND SIMULATION

The schematic representation of the numerical experiment system is shown in Fig. 1. Except for the particle condition, the configurations and simulation methods used were identical to those presented by Yamamoto *et al.* [12]. The test cell was a rectangular vessel with depth $D = 3$ mm, width $T = 2D$, and height $L = 8D$. Stationary suspensions were initially installed on the upper and lower sides. The liquid properties were set similar to those of silicone oil (mass density $\rho_l = 972$ kg/m³ and dynamic viscosity $\mu_l = 0.1$ Pa s). For the vessel in this study, Yamamoto *et al.* [12] found $2K = 0.465$ in Eq. (8). The initial heights of upper and lower suspensions were both $3.45D$. The particle properties were varied, as shown in

Tables I–IV (full information is provided in Ref. [17]). For all cases, particle terminal velocities were set to $U_{\text{St1}} = 4.000 \times 10^{-5}$ m/s, and the precision of terminal velocities was kept in almost four significant digits by adjusting the particle mass density.

As in previous studies [11,12,16,18], we employed the Lagrangian tracking of individual particles with two-way coupling using a point-force model by ignoring particle inertia for a very small Stokes number. In the present simulations, we must treat both mixing by differential settling and by hydrodynamic interactions due to large and long-ranged velocity fluctuations [3]. Both effects can be naturally contained in this two-way coupling point-force Lagrangian method, which is an extension of the approach fully validated by comparing with experimental measurements [11,16]. The particle velocity was determined by the interpolated liquid velocity at the particle position plus its terminal velocity in the gravitational direction, and the particle position was subsequently updated using the second-order Adams-Bashforth method. The liquid was incompressible, and its motion was described by the continuity and the two-way-coupled Navier-Stokes equations. Those equations were spatially discretized using the second-order central finite-difference method. The simplified marker and cell algorithm were used to link pressure and advance in time.

The numbers of grid points for D , T , and L were set to 8, 16, and 64, respectively. The time step was set to a range of $1\text{--}2.5 \times 10^{-5}$ s. The particle and liquid velocities were set to zero as initial conditions, and the particle positions were determined using random numbers. For liquid motion, the no-slip and no-permeable conditions were applied to all external boundaries. For the particle motion, the perfect elastic with no-friction conditions was applied to external boundaries except for the bottom wall. At the bottom wall, particles were deposited with zero repulsion coefficient. To avoid interfering with the mixing of suspensions, the top wall was slightly sepa-

TABLE III. Suspension conditions for test 3. Subscripts 1 and 2 represent upper and lower suspensions, respectively.

	Y_m	C_{mod1}	C_{mod2}	d_{p1}	d_{p2}	ρ_{p1}	ρ_{p2}	ϕ_1	ϕ_2	ρ_{s1}	ρ_{s2}	$U_{\text{St2}}/U_{\text{St1}}$
3-A- α	100	Identical to 1-A- α						0.015	0.0067	1074	1032	1
3-A- β		Identical to 1-A- β										
3-B- α	50	11.00	8.4	33.4	29.3	7557	9528	0.015	0.0067	1074	1032	1
3-B- β					80.2		2116.58		0.05			
3-C- α	5	11.00	10.8	33.4	29.3	7557	9528	0.015	0.011 06	1074	1070	1
3-C- β					62.3		2867		0.05			

TABLE IV. Suspension conditions for test 4. Subscripts 1 and 2 represent upper and lower suspensions, respectively.

	Y_m	$C_{\text{mod}1}$	$C_{\text{mod}2}$	d_{p1}	d_{p2}	ρ_{p1}	ρ_{p2}	ϕ_1	ϕ_2	ρ_{s1}	ρ_{s2}	U_{St2}/U_{St1}
4-A- α	5	11.00	7.61	33.4	29.3	7557	180 80	0.015	0.005 53	1074	1070	2
4-A- β					62.3		4758		0.025			
4-B- α	5					Identical to 3-C- α						1
4-B- β												
4-C- α	5	11.00	15.2	33.4	29.3	7557	5251	0.015	0.0221	1074	1070	0.5
3-C- β					44.1		2863		0.05			

rated from the top of the upper-suspension packed region (i.e., there is a pure liquid region between the top wall and the upper suspension). For the time step, because of the large viscosity, the time step must be small to obtain a convergent solution even if the implicit solution method is used for the viscous term. The time step was adjusted according to the particle conditions because the convergence speed varies with particle concentration. A suitable implementation was discussed by Yamamoto *et al.* [16] and validated by comparing the results with the experimentally obtained values reported by Mori *et al.* [11]. The grid resolution dependency was verified in Yamamoto *et al.* [12].

III. RESULTS AND DISCUSSION

The first set of numerical experiments (test 1) were conducted with fixed parameters as large as $Y_m = 100$ with $U_{St2}/U_{St1} = 1$ and various collectivities C_{mod} shown in Table I. The difference between α and β in each case is the lower particle diameter; the lower particle is smaller than the upper particle in α , while the lower particle is larger than the upper particle in β for the same collectivity, $C_{\text{mod}2}$.

Figure 2 shows the instantaneous particle distribution at time $t = 10$ s in the center plane with depth $0.1D$ for the cases in Table I. In all cases, we found the fingering settling with a typical mushroom shape, as commonly found in single-mode Rayleigh-Taylor mixing. The mixing behaviors of these six cases with $Y_m = 100$ composed of different collectivities and

particle diameter conditions were similar. We also examined the mixing rates dZ_{mix}/dt from the linearly increasing part of Z_{mix} and found that they were almost the same.

The second set of numerical experiments (test 2) was conducted with fixed $Y_m = 100$ with various U_{St2}/U_{St1} , as shown in Table II. For the vessel in this study, $2K = 0.465$ in Eq. (8); therefore the mixing rate dZ_{mix}/dt for $Y_m = 100$ can be estimated as approximately 50 times the terminal velocity U_{St1} .

Figure 3 shows the instantaneous particle distribution at time $t = 10$ s for the cases in Table II. In all cases, we found the typical-mushroom-shaped fingering settling. The mixing behaviors of these six cases with $Y_m = 100$ and different lower suspension conditions were similar. In particular, the upper particle conditions and even the initial particle positions in those six cases were completely the same; thus, the characteristics (rightward curved settling) of the upper suspensions were also similar. The microscopic (individual particle-scale) mixing due to the terminal velocity difference was not found, even in those magnified images because the macroscopic (vessel-scale) mixing rate was much larger (about 50 times) than the terminal velocity. We found that the mixing rates for those cases were almost the same, as shown later.

The third set of numerical experiments (test 3) was conducted with various Y_m with the same upper suspension, as shown in Table III.

Figure 4 shows the instantaneous particle distribution for the cases in Table III. For $Y_m \geq 50$, we found the typical-mushroom-shaped fingering settling but not microscopic mixing. However, for $Y_m = 5$, such a typical settling was not

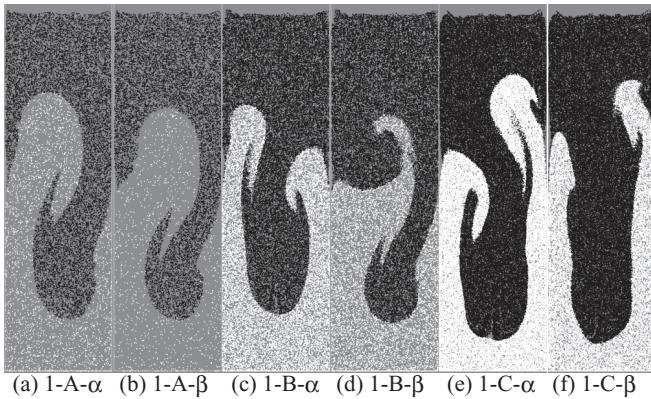


FIG. 2. Center-plane particle distribution at 10 s of test 1, where $Y_m = 100$ with the same terminal velocity cases, in the center-plane region with a depth of $0.1D$ ($0.45D < y < 0.55D$). Black dot: upper particle. White dot: lower particle. The dot size does not reflect the size of the particle, and upper pure liquid regions are cut out.

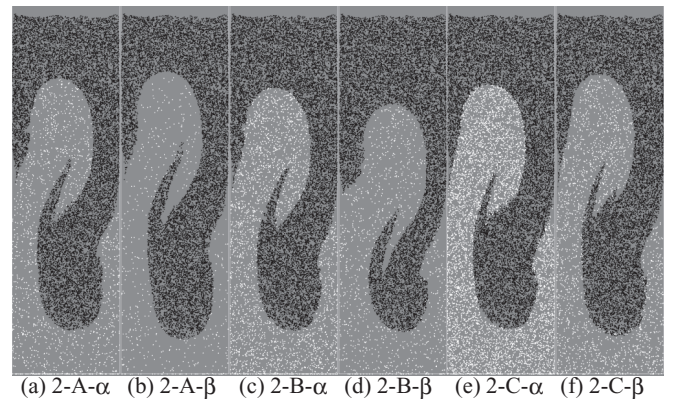


FIG. 3. Center-plane particle distribution at 10 s of test 2, where $Y_m = 100$ with different terminal velocities of lower particles (see the caption of Fig. 2).

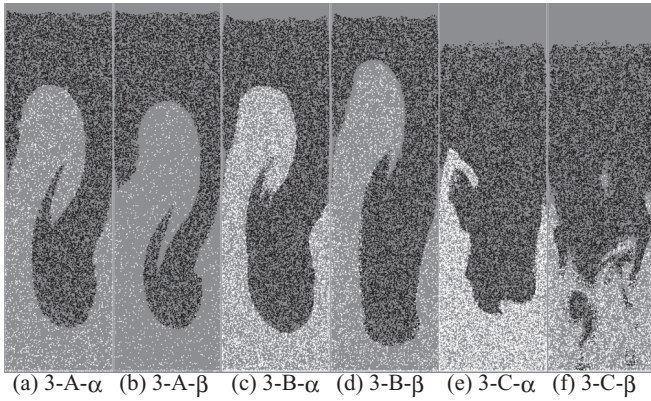


FIG. 4. Center-plane particle distribution of test 3, $Y_m = 100$ (A, $t = 10$ s), $Y_m = 50$ (B, $t = 17.5$ s), and $Y_m = 5$ (C, $t = 50$ s) with the same terminal velocity (see the caption of Fig. 2).

observed, and complex settling patterns were found. In this test, the upper particle conditions were completely the same as those of the initial positions in these six cases; however, the characteristics of settling behaviors and the mixing rate were completely different due to the difference in the lower suspensions' collectivities. The larger the lower suspension's collectivity was, the smaller the apparent density difference between the upper and lower suspensions was. For Rayleigh-Taylor mixing of two immiscible fluids without interfacial tension, the small density difference just retards the growth of fingering settling; however, particles individually settle with a relative speed to the liquid in the gravitational mixing of stratified suspensions. Thus, the instability at the suspensions' interface cannot grow enough, and the dominantly grown wavelength becomes different from the wavelengths of other Y_m cases. The details for low Y_m number cases are discussed in the following test.

The fourth set of numerical experiments (test 4) was conducted with fixed $Y_m = 5$ with the same upper suspension, as shown in Table IV. Using Eq. (8), the macroscopic mixing rate for $Y_m = 5$ can be estimated as $2U_{St1}$, indicating that the macroscopic mixing rate is in the same order of the micro-

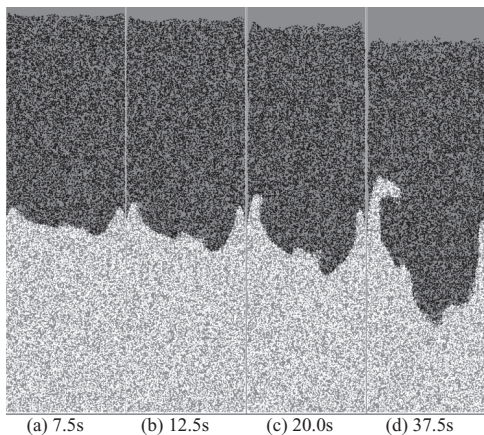


FIG. 5. Mixing behavior of test 4-B- α , where $Y_m = 5$ with the same terminal velocity, large particles on small particles in 0.1D depth center plane.

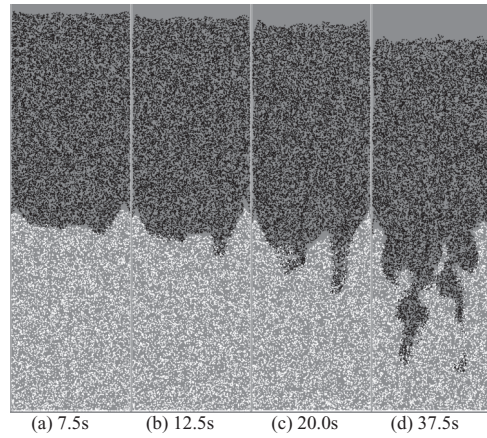


FIG. 6. Mixing behavior of 4-B- β , small particles on large particles in 4-B.

scopic mixing rate. Thus, the lower particles move away from the upper suspension in case 4-A, and the upper particles plunge into the lower suspension in case 4-C.

Figures 5 and 6 show the mixing behaviors for cases 4-B in Table IV corresponding to the temporal development of Figs. 4(e) and 4(f). For these cases, the apparent density

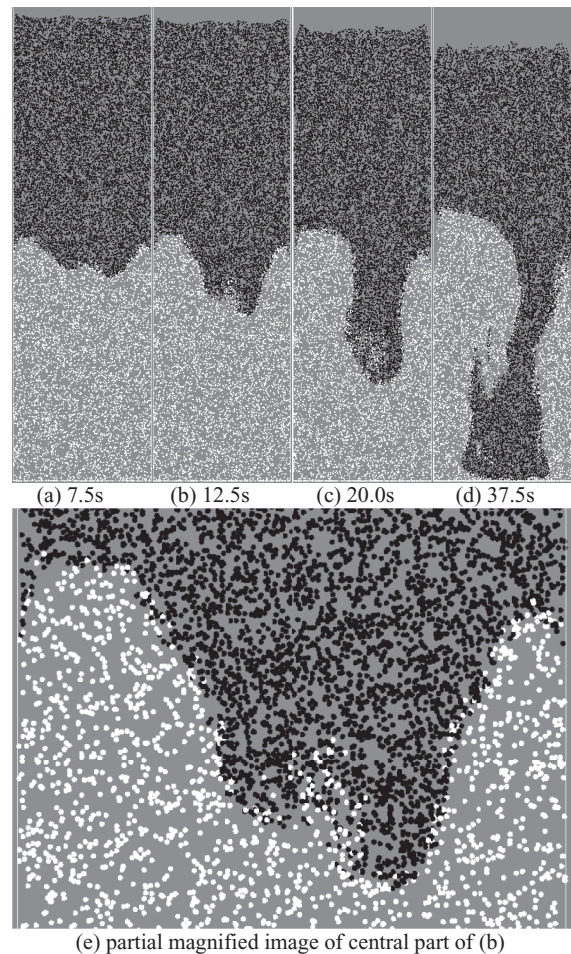


FIG. 7. Mixing behavior of test 4-C- α , where $Y_m = 5$ with $U_{St2} = 0.5U_{St1}$ cases, large particles on small particles.

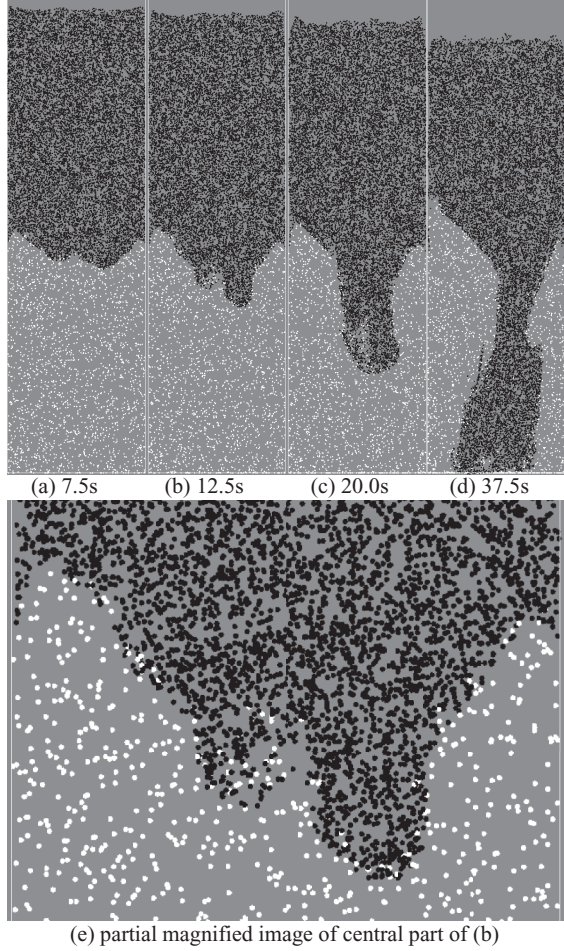


FIG. 8. Mixing behavior of test 4-C- β , small particles on large particles in 4-C.

difference between the upper and lower suspensions is very small ($1074\text{--}1070\text{ kg/m}^3$); thus, the instability at the suspensions' interface grows very slowly. Further, particles in those suspensions settle down at the terminal velocity individually by dragging the surrounding liquid. However, since the liquid movement is constrained by volume conservation, a complex mixing behavior occurs. In these cases, due to the same terminal velocity, $U_{S12} = U_{S11}$, microscopic mixing does not occur. The macroscopic mixing behaviors without mushroom-type fingering are found in low Y_m with $U_{S12}/U_{S11} = 1$.

Figures 7 and 8 show the mixing behaviors for cases 4-C in Table IV. For these cases with the same Y_m as in test 4-B, the apparent density difference between the upper and lower suspensions is very small. However, the upper particles settle faster than the lower particles since $U_{S11} = 2U_{S12}$; thus, the microscopic mixing occurs at the suspensions' interface. Then, the interface instability growth is promoted by the increasing apparent density of the mixed region from ρ_{s1} to ρ_{mix} , where

$$\begin{aligned}\rho_{\text{mix}} &= (\phi_1 \rho_{p1} + \phi_2 \rho_{p2}) + (1 - \phi_1 - \phi_2) \rho_l \\ &= \rho_{s1} + \phi_2 (\rho_p - \rho_l).\end{aligned}\quad (9)$$

As a result, the fingering settling behaviors are observed for both α and β cases, and the mixing rate becomes the sum of the microscopic and macroscopic mixing contributions.

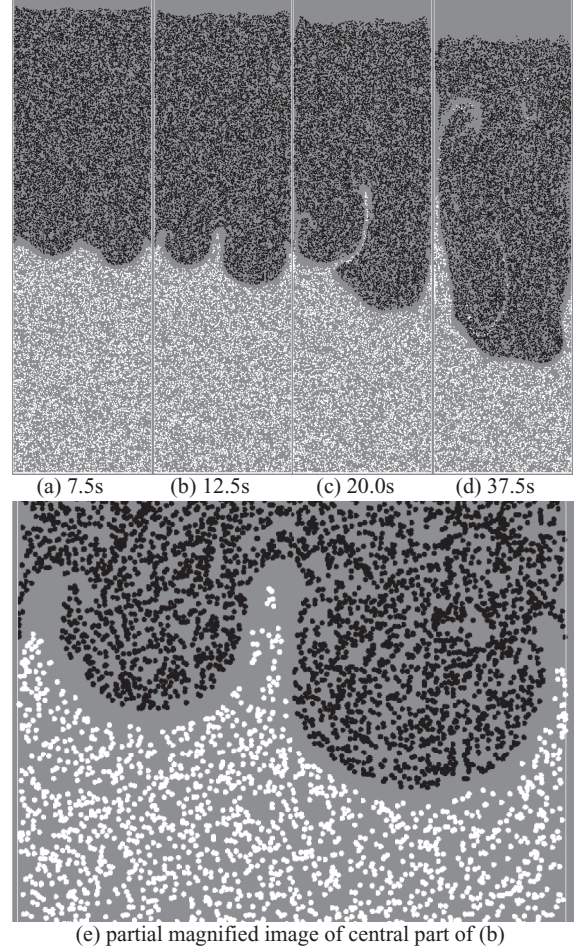


FIG. 9. Mixing behavior of test 4-A- α , where $Y_m = 5$ with $U_{S12} = 2U_{S11}$ cases, large particles on small particles.

Figures 9 and 10 show the mixing behaviors for cases 4-A in Table IV. For these cases with the same Y_m as in the other test 4, the apparent density difference between the upper and lower suspensions is very small. If one tries conducting the real experiments for this condition, such a density difference may be hardly controlled and the densities may be approximately equal. Therefore, the instability at the suspensions' interface grows very slowly. Furthermore, the lower particles settle faster than the upper particles because $U_{S12} = 2U_{S11}$, and the pure liquid layer is generated between the upper and lower suspensions. At the interface between the pure liquid layer and the lower suspension, the interface proceeds in the direction of flattening due to gravitationally stable conditions. Thus, the growth of interface instability between the upper suspension and the pure liquid layer is inhibited by the flattened lower interface. Then, the upper suspension settles with the flattened interface (two flattened fingers observed in both Figs. 9 and 10 push down the lower suspension). Because of volume conservation, the lower suspension cannot help but jet up somewhere. Thus, we obtained jet flow in the central part of the interface in both Figs. 9 and 10. As a result, the mixing rate becomes larger than test 4-B and 4-C cases because of jetting. However the total mixing state may be, the mixing rate is large in small Y_m with $U_{S12} > U_{S11}$ (the mixing rate

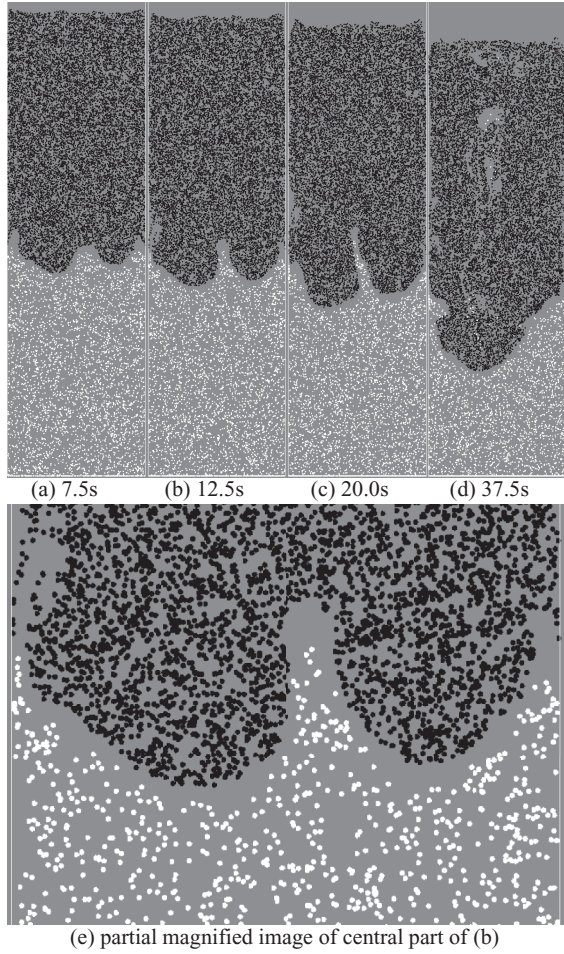


FIG. 10. Mixing behavior of test 4-A- β , small particles on large particles in 4-A.

is defined by the vertical distance between the bottom-most particle of the upper suspension and the top-most particle of the lower suspension). Overall, the observed behaviors are very interesting from a physical point of view.

The mixing rates were calculated by linear fitting, as reported by Yamamoto *et al.* [12], for the results of the present

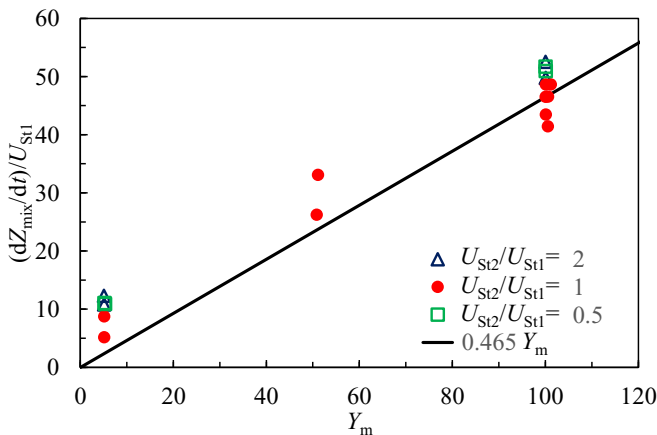


FIG. 11. Mixing rates obtained by numerical experiments with Eq. (8).

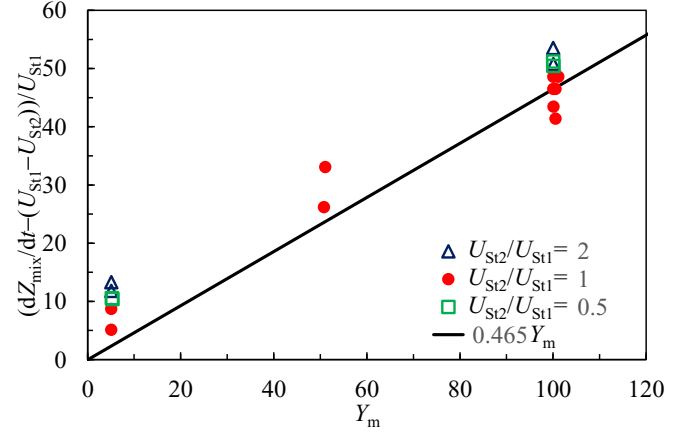


FIG. 12. Strict version of mixing rates with Eq. (10).

numerical tests. The mixing rates are plotted in Fig. 11. In cases with terminal velocity differences, the mixing rate may tend to be larger than that of the same terminal velocity case.

In Yamamoto *et al.* [12], the mixing rate at $Y_m = 0$ was not considered in Eq. (8). For the limit of $Y_m \rightarrow 0$, the mixing rate should approach the difference in the terminal velocities; thus, the strict version of the mixing rate is described as follows:

$$\left[\frac{dZ_{\text{mix}}}{dt} - (U_{St1} - U_{St2}) \right] \frac{1}{U_{St1}} = 2KY_m. \quad (10)$$

The strict version of the mixing rates (corresponding to the macroscopic mixing rates) is plotted in Fig. 12. The mixing rates of the stratified suspension produced by the present simulation method vary with the initial conditions in the range of about $10U_{St1}$, even for the same Y_m . So, the vertical shift with the above strict consideration $U_{St1} - U_{St2}$ and the complex microscopic mixing effect observed in $Y_m = 5$ conditions are within a reasonable range. Thus, the mixing rate equation concerning the nondimensional number Y_m proposed by Yamamoto *et al.* [12] [Eq. (8)] can still be effectively used for rough estimations.

IV. CONCLUSION

Based on the mixing rate estimation equation proposed in our previous work [12], we conducted numerical experiments to study the effects of modified collectivity and the particle terminal velocity ratio, the components of the nondimensional number Y_m , on the mixing behavior of stratified suspensions.

For $Y_m = 100$, macroscopic mixing due to gravitational instability is dominant, and the different values of components for the same Y_m do not affect the mixing behavior. In those cases, microscopic mixing due to the terminal velocity difference cannot be observed.

For $Y_m = 5$, where the macroscopic mixing rate is in the same order as the microscopic mixing rate, when the upper and lower terminal velocities are the same, instability near the suspension interface grows very slowly because of the small apparent density difference, and particles settle individually relative to the liquid; thus, settling as small pieces is observed unlike in the Rayleigh-Taylor mixing of two immiscible fluids. When the upper terminal velocity is larger than

the lower terminal velocity, microscopic mixing produces a high-apparent-density region, promoting instability near the suspension interface. When the lower terminal velocity is larger than the upper terminal velocity, the pure liquid layer is produced between two suspensions, and the gravitationally stable lower-side interface prevents the growth in the variation of the gravitationally unstable upper-side interface. Because of the volume conservation of the liquid and the force exerted by the flattened interface of the upper suspension, the jetting up of the lower suspension is formed. Although mixing rates vary depending on such mixing behaviors, macroscopic mixing rates essentially vary with a slight difference in the suspension setting. Thus, the equation proposed in the previous work [12] reasonably estimates the mixing behaviors of stratified suspensions.

In a system of suspensions of approximately equal apparent density in contact with the top and bottom, one would normally expect no mixing if the terminal velocity of

the lower particle is greater than that of the upper particle because the lower particles move away from the upper particles. However, if the particle concentration changes slightly and the apparent density of the upper suspension becomes slightly (even less than 1%) greater than that of the lower suspension, an unexpected result is observed where a jet suddenly mixes out of an unmixing situation, as described above. This is a very valuable finding. The knowledge of this unexpected mixing is critical for spontaneous mixing and active control of mixing, such as preventing the mixing of things that should not be mixed or mixing things that are difficult to mix in practical applications.

ACKNOWLEDGMENT

This study was supported by JSPS KAKENHI Grant No. 19H02058.

-
- [1] J. Thakurta, E. M. Ripley, and C. Li, Geochemical constraints on the origin of sulfide mineralization in the Duke Island Complex, southeastern Alaska, *Geochem. Geophys. Geosyst.* **9**, Q07003 (2008).
 - [2] P. N. Segrè, E. Herbolzheimer, and P. M. Chaikin, Long-Range Correlations in Sedimentation, *Phys. Rev. Lett.* **79**, 2574 (1997).
 - [3] É. Guazzelli and J. Hinch, Fluctuations and instability in sedimentation, *Annu. Rev. Fluid Mech.* **43**, 97 (2011).
 - [4] R. H. Davis and A. Acrivos, Sedimentation of noncolloidal particles at low Reynolds numbers, *Annu. Rev. Fluid Mech.* **17**, 91 (1985).
 - [5] C. Völtz, W. Pesch, and I. Rehberg, Rayleigh-Taylor instability in a sedimenting suspension, *Phys. Rev. E* **65**, 011404 (2001).
 - [6] F. Blanchette and J. W. M. Bush, Particle concentration evolution and sedimentation-induced instabilities in a stably stratified environment, *Phys. Fluids* **17**, 073302 (2005).
 - [7] S. Harada, T. Mitsui, and K. Sato, Particle-like and fluid-like settling of a stratified suspension, *Eur. Phys. J. E* **35**, 1 (2012).
 - [8] J. M. Nitsche and G. K. Batchelor, Break-up of a falling drop containing dispersed particles, *J. Fluid Mech.* **340**, 161 (1997).
 - [9] G. Machu, W. Meile, L. C. Nitsche, and U. Schafflinger, Coalescence, torus formation and breakup of sedimenting drops: experiments and computer simulations, *J. Fluid Mech.* **447**, 299 (2001).
 - [10] B. Metzger, M. Nicolas, and É. Guazzelli, Falling clouds of particles in viscous fluids, *J. Fluid Mech.* **580**, 283 (2007).
 - [11] M. Mori, T. Tai, K. Nishimura, S. Harada, and Y. Yamamoto, Possibility of non-Fickian mixing at concentration interface between stratified suspensions, *J. Colloid Interface Sci.* **571**, 13 (2020).
 - [12] Y. Yamamoto, K. Yamada, Y. Tanaka, and S. Harada, Macroscopic and microscopic hydrodynamic mixing of stratified suspensions, *Phys. Rev. E* **104**, 025111 (2021).
 - [13] R. C. Clift, B. J. Grace, and M. E. Weber, *Bubbles, Drops, and Particles* (Academic Press, New York, 1978).
 - [14] S.-I. Sohn, Effects of surface tension and viscosity on the growth rates of Rayleigh-Taylor and Richtmyer-Meshkov instabilities, *Phys. Rev. E* **80**, 055302(R) (2009).
 - [15] R. Zanella, G. Tegze, R. Le Tellier, and H. Henry, Two- and three-dimensional simulations of Rayleigh-Taylor instabilities using a coupled Cahn-Hilliard/Navier-Stokes model, *Phys. Fluids* **32**, 124115 (2020).
 - [16] Y. Yamamoto, F. Hisataka, and S. Harada, Numerical simulation of concentration interface in stratified suspension: continuum-particle transition, *Int. J. Multiphase Flow* **73**, 71 (2015).
 - [17] See Supplemental Material at <http://link.aps.org/supplemental/10.1103/PhysRevE.106.045109> for full information of suspensions' data.
 - [18] T. Bosse, L. Kleiser, C. Härtel, and E. Meiburg, Numerical simulation of finite Reynolds number suspension drops settling under gravity, *Phys. Fluids* **17**, 037101 (2005).